A&A 404, 133–144 (2003)
DOI: 10.1051/0004-6361:20030435

Astronomy & Astrophysics

The spectral-curvature parameter: An alternative tool for the analysis of synchrotron spectra

B. W. Sohn[1,2], U. Klein[2], and K.-H. Mack[2,3,4]

[1] Max-Planck-Institut für Radioastronomie, Auf dem Hügel 69, 53121 Bonn, Germany
[2] Radioastronomisches Institut der Universität Bonn, Auf dem Hügel 71, 53121 Bonn, Germany
[3] ASTRON/NFRA, Postbus 2, 7990 AA Dwingeloo, The Netherlands
[4] Istituto di Radioastronomia del CNR, via P. Gobetti 101, 40129 Bologna, Italy

Received 23 August 2001 / Accepted 17 March 2003

Abstract. A new intuitive tool for the analysis of synchrotron spectra is presented. The so–called *Spectral Curvature Parameter (SCP)*, when plotted versus the high–frequency spectral index ($\alpha_{\rm high}$) of synchrotron sources, provides crucial parameters on the continuum spectrum of synchrotron radiation without the more complex modeling of spectral ageing scenarios. An important merit of the *SCP*-α diagram, in respect to the conventional colour-colour diagram (i.e. α-α diagram), is the enhanced reliability of extracting multiple injection spectra, $\alpha_{\rm inj}$. Different from the colour-colour diagram, tracks of different $\alpha_{\rm inj}$s, especially when the synchrotron particles are young, exhibit less overlap and less smearing in the *SCP*-α diagram. Three giant radio galaxies (GRGs) and a sample of Compact steep spectrum (CSS) souces, which are particularly suitable for this kind of analysis, are presented. GRGs exhibit asymmetries of their injection spectral indices $\alpha_{\rm inj}$ in the *SCP*-$\alpha_{\rm high}$ diagram. The obtained $\alpha_{\rm inj}$s and the trends in the sources are cross-checke with the literature and show remarkable confidence. Besides the spectral steepening which is well understood in the framework of synchrotron ageing models, spectral flattening is prominent in the radio lobes. The spectral flattening is a clue to efficient re-acceleration processes in the lobes. This implies that interaction with the surrounding intergalactic or intra-cluster medium is an important characteristic of GRGs. In the SW lobe of DA 240, there is a clear sign of CI and KP/JP bifurcation at the source extremity. This indicates a highly relativistic energy transportation from the core or in situ acceleration in this typical FR I lobe. Our analysis proves, if exists, KP spectra imply the existence of strong $B_{\rm sync}$ field with $B_{\rm sync} > B_{\rm CMB}$. In the CSS sources, our result confirms the CI model and $B_{\rm sync} \gg B_{\rm CMB}$. The synchrotron self-absorption is significant in the CSS sample.

Key words. galaxies: jets – radio continuum: galaxies – methods: data analysis

1. Introduction

Spectra of synchrotron sources from the radio to the X-ray regime reflect the energy distribution of relativistic particles, i.e. electrons whose energy distributions obey a power-law. In general, the synchrotron emissivity also follows a power-law (Pacholczyk 1970). While the conventional spectral indices only provide the spectral slope between the two observing frequencies, a multi-frequency data set can also disclose spectral curvatures over a larger frequency range. The significance of the shape of synchrotron spectra has been underlined early on by Kardashev (1962); Pacholczyk (1970); Pacholzcyk (1977); Jaffe & Perola (1973), who were among the first to describe and apply synchrotron loss models to flux densities obtained at several frequencies.

It is obvious that the information on the spectral shape of a source under the effects of ageing, adiabatic expansion etc. provides an important tool for understanding source evolution. If the injection of relativistic particles following a power-law is restricted to a certain region – the cores and/or hot spots of radio galaxies – and if the observation is performed with appropriate resolution, one can detect regional variations of spectral curvature by means of the above-mentioned physical processes. Since synchrotron and Inverse Compton losses are the main energy dissipation processes in radio galaxies, in particular at high and intermediate radio frequencies (>1 GHz), large efforts have been made to explain the variation of spectral curvatures – often by modeling two-frequency data – of radio galaxies with the synchrotron ageing theory (e.g. Alexander & Leahy 1987; Alexander 1987; Klein et al. 1995; Feretti et al. 1998; Murgia et al. 1999). A proper determination of parameters like the injection spectral index $\alpha_{\rm inj}$ (the spectrum of the electron distribution immediately after acceleration, $N(E) \propto E^{-p}$, $\alpha_{\rm inj} = (p-1)/2$ or the break frequency $\nu_{\rm br}$, the frequency at which spectral steepening occurs can be obtained with a spectral ageing analysis (e.g. Carilli et al. 1991; Mack et al. 1998; Murgia et al. 1999). This requires, however, the fitting of appropriate models with several parameters, thus high-quality

Send offprint requests to: B. W. Sohn,
e-mail: bwsohn@mpifr-bonn.mpg.de

measurements at many fequencies with a good signal-to-noise ratio are essential.

In order to fit synchrotron and Inverse-Compton losses, three models are widely used: The continuous injection (CI) model (Pacholczyk 1970) assumes a mixture of electron populations of various synchrotron ages. In this model, permanent replenishment of fresh particles is assumed so that the injection spectral index steepens to its final value of $\alpha_{\rm inj}$ + 0.5 beyond the break frequency. The Kardashev-Pacholczyk (KP) model (Kardashev 1962; Pacholczyk 1970) merely includes a single injection of power-law distributed electrons. The pitch angles of the electrons are assumed to be constant with time. The high-frequency slope in this model is $\frac{4}{3}\,\alpha_{\rm inj} + 1$. The Jaffe-Perola (JP) model (Jaffe & Perola 1973) incorporates – similar to KP – a single injection but permits permanent pitch angle isotropization. Beyond the break frequency this model leads to an exponential steepening of the high-frequency spectrum. A sketch of the different tracks of the various ageing models in the classical $\log(S) - \log(\nu)$ space can be found in the work of Carilli et al. (1991, see their Fig. 1).

In many cases the spectral ageing analysis yielded significant results. However, high-resolution multi-frequency studies of two prototypical nearby radio galaxies – 3C 449 (FR I type) by Katz-Stone & Rudnick (1997) and Cygnus A (FR II type) by Carilli et al. (1991), show trends that cannot be explained by the synchrotron ageing theory alone. The first problem is that jets and lobes (3C 449), and hot-spots and lobes (Cygnus A) have different injection spectra. The second problem to be dealt with is that of the microscopic physical conditions. While possible physical conditions such as turbulent magnetic fields and inverse-Compton scattering by cosmic microwave background photons favour the pitch-angle isotropized (JP) model, the observational results appear to support the constant pitch angle (KP) model. This could mean that the nature of the spectral curvature is more complex than expected from the synchrotron ageing theory alone.

Carilli & Barthel (1996) have pointed out the necessity of an appropriate empirical analysis that is not tied to any theoretical model in order to find the real trends in sources. Here we present a new method which can fulfill this requirement. It also aims at a quick determination of the injection spectral index and the best suited model to fit the observed spectrum. It fills the gap between the simple spectral index study and the much more complex spectral ageing analysis. It is also suited to provide first guesses of the parameters to be fit in a spectral ageing analysis, therefore making the fit procedure less susceptible to local minima in the error space.

2. The spectral curvature parameter-α diagram

This method is based on the so-called spectral curvature parameter (*SCP*). It is defined as

$$SCP \equiv \frac{\alpha_{\rm high} - \alpha_{\rm low}}{\alpha_{\rm high} + \alpha_{\rm low}}.$$

When displayed as a function of the spectral index α with

$$I_\nu \propto \nu^{-\alpha},$$

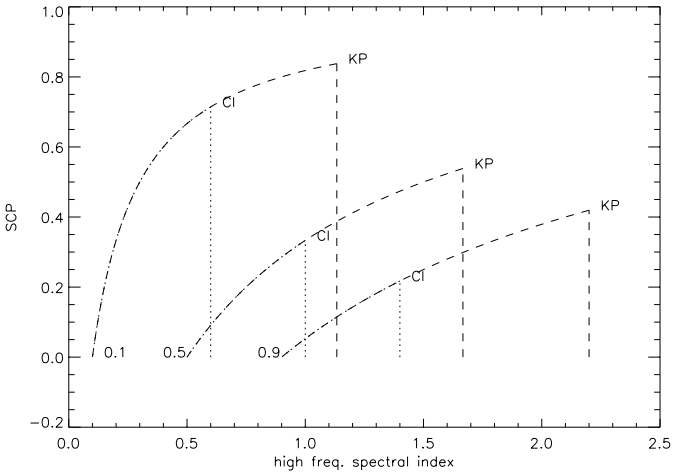

Fig. 1. Schematic *SCP*–$\alpha_{\rm high}$ diagram of power-law injection spectra, $\alpha_{\rm inj} = 0.1, 0.5, 0.9$, undergoing synchrotron losses. The numbers represent the injection spectral index of each line. Along the dash-dotted curves, all models, i.e. CI, KP and JP are possible. At the maximum *SCP* values of the CI models the tracks between CI (dotted lines) and KP/JP (dashed lines) split at the points marked "CI". Along the dashed curves the KP and JP models are possible. At $SCP_{\rm max}$ of the KP model (marked "KP") the KP (dashed straight lines) and JP models (imaginary curves approaching $SCP = 1$) take separate tracks. The break frequency, $\nu_{\rm br}$, reaches the low frequency regime such that $\nu_1 \geq \nu_{\rm br} \geq \nu_2$ where ν_1, ν_2 are the frequencies used for the estimation of $\alpha_{\rm low}$. The KP spectra will fall vertically to $SCP = 0$, since $\alpha_{\rm high} = \alpha_{\rm KP,br} = 4/3\alpha_{\rm inj} + 1$. The JP high-frequency tail falls off exponentially beyond the break frequency in the $\log(S_\nu) - \log(\nu)$ diagram, therefore the track will approach asymptotically $SCP = 1$ in the *SCP*-$\alpha_{\rm high}$ regime. Tracks of these most common synchrotron ageing models in the $\log(S_\nu) - \log(\nu)$ parameter space are sketched by Carilli et al. (1991).

the *SCP* indicates how the spectrum evolves, starting from its pure power-law. As $\alpha_{\rm high}$ is more sensitive to both spectral steepening and spectral flattening than $\alpha_{\rm low}$ (Pacholczyk 1970; Eilek & Hughes 1991; Carilli et al. 1991), we employ $\alpha_{\rm high}$ as the counter axis of *SCP*. Though the classical $\log(S_\nu) - \log(\nu)$ diagram is the best way to test ageing models for a single-spectrum population, it is not a straight-forward tool to unveil different trends in an extended source. It is here where the *SCP*-α diagram has its power. Each spectrum is represented by a point in the *SCP*-α plane, and a lot of spectra from an extended source can be drawn in this plane.

Figure 1 illustrates the schematic tracks of the power-law spectra undergoing synchrotron ageing. More realistic simulations of *SCP*–α diagram including the Inverse Compton equivalent field of Cosmic Microwave Background radiation, i.e. $B_{\rm CMB}$, are presented in what follows. The dash-dotted curved lines represent tracks where the break frequency has not yet reached the low-frequency regime (i.e. where $\alpha_{\rm low}$ is determined). The CI, KP and JP models produce different *SCP* ranges. This makes it easy to distinguish between the different models in the *SCP*-$\alpha_{\rm high}$ plane. Different injection spectral indices also follow different tracks.

Since both the CI and the KP model predict a power-law spectrum also beyond the break frequency, namely the

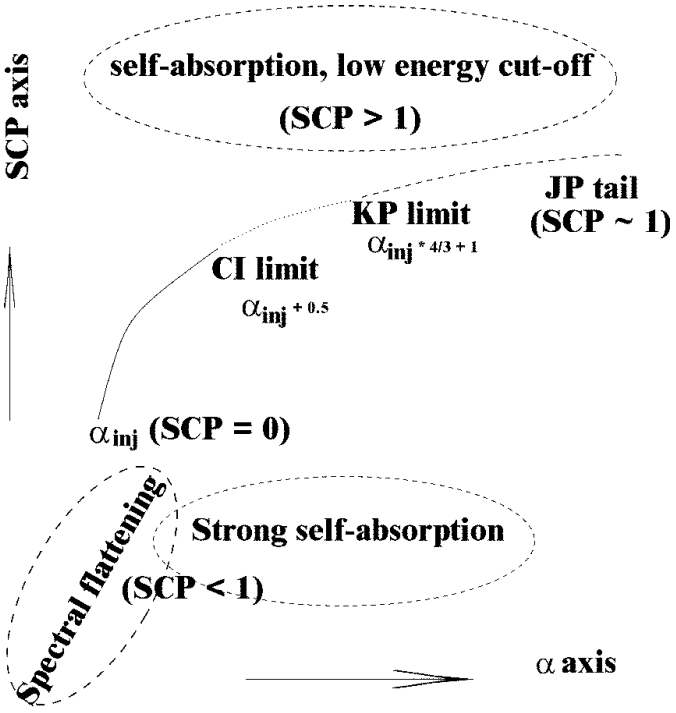

Fig. 2. Schematic diagram of a synchrotron source with a given injection spectrum and with various processes that affect the spectral curvature. In this sketch, the classical pitch angle models, i.e. KP and JP are considered.

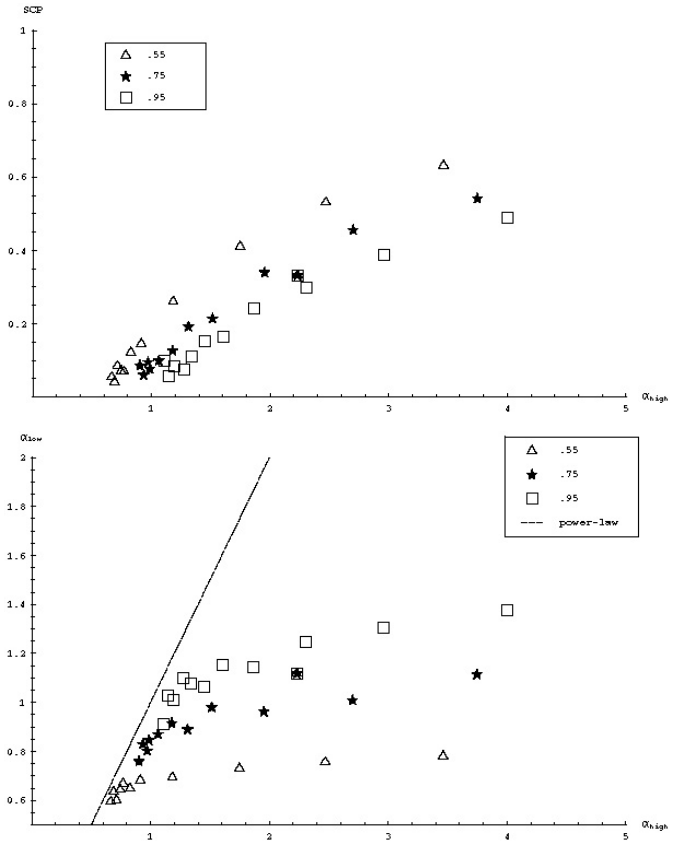

Fig. 3. Comparison between *SCP*-α and the colour-colour diagram with $B_{\rm sync}$ = 6.0 μG, $B_{\rm CMB}$ = 3.2 μG and JP model. The two field strengths are simply additive in JP model, since they both are isotropic. The frequency intervals were selected to be similar to standard observing frequencies in the classical radio regime. Open triangles are the result with $\alpha_{\rm inj}$ = 0.55. Filled stars are the result with $\alpha_{\rm inj}$ = 0.75. Open squares are the result with $\alpha_{\rm inj}$ = 0.95. The dotted line in the Colour-Colour diagram is $\alpha_{\rm low}$ = $\alpha_{\rm high}$ line, i.e. a pure power-law while in the *SCP*-α diagram this corresponds to *SCP* = 0. In the simulation, we assumed the low energy cut-off, E_0, and the high energy cut-off by CMB photons. The energy range is binned in 200 bins. At given frequencies, the synchrotron radiation contribution from each bin is calculated.

so-called broken power-law (Eilek & Hughes 1991), we can calculate the maximum *SCP*s in these cases. For $\alpha_{\rm inj}$ = 0.5, these are $SCP_{\rm CI,max}$ ~ 0.33 and $SCP_{\rm KP,max}$ ~ 0.54. In contrast, the high-frequency part of the JP model has a non-power-law curvature, viz. an exponential one. Therefore, the tracks of JP spectra asymptotically approach *SCP* = 1.0. In any case, $\alpha_{\rm h} > (\frac{4}{3})\alpha_{\rm inj} + 1$ is predicted by the JP model only.

2.1. SCP-α diagram and colour-colour diagram

An advantage of the *SCP*-α diagram with respect to the colour-colour diagram (Katz-Stone et al. 1993), is seen when the source has multiple $\alpha_{\rm inj}$s. As predicted in the particle ageing theory, the track of an aged $\alpha_{\rm inj}$ do not leave immediately the $\alpha_{\rm low}$ = $\alpha_{\rm high}$ line (see Fig. 3). Because of the overlap of the $\alpha_{\rm low}$ = $\alpha_{\rm high}$ line and the spread of points parallel to it in the colour-colourdiagram (hereafter C–C diagram), trends in the source can not be easily identified. We emphasize that there are model dependent aspects in the spectral tomography or the classical synchrotron ageing analysis, (e.g. Alexander & Leahy 1987; Murgia et al. 1999).

For example, the synchrotron ageing analysis can hardly achieve a pixel-to-pixel study. The synchrotron ageing analysis is therefore done in a way with certain subdivided integrated areas. As a property of the integration, the obtained $\alpha_{\rm inj}$ is strongly biased by bright structures in these areas. The spectral tomography aimed at solving this problem. This technique isolates from an assumed or known $\alpha_{\rm inj}$ component a "different" component. The $\alpha_{\rm inj}$ of this "different" component is not directly obtained in the spectral tomography. The spectral tomography with multiple $\alpha_{\rm inj}$s could be much more complex than the classical synchrotron ageing analysis (Katz-Stone & Rudnick 1994). The tool suggested here will extract $\alpha_{\rm inj}$s without the bias due to bright structures and without complex tomographical mapping. It can serve as a "precensor", such as to select the area of integration in the synchrotron ageing analysis correctly, thus providing quite reliable physical parameters.

The clear bifurcations on the *SCP*-α diagram, between CI and KP/JP and between KP and JP, are further merits of the *SCP*-α diagram. On the other hand, the tracks of the different models beyond the $\nu_{\rm br}$ show overlaps on the C–C diagrams.

In both cases, i.e. CI and KP, straight vertical lines arise, while in the KP/JP and JP case the original curves are maintained. This fact makes the selection of the proper ageing model easier than in the C–C diagram. Of course, under the influence of CMB, this last argument is only true if $B_{\rm sync}$ is (much) stronger than $B_{\rm CMB}$. The weak point of both, the C–C diagram

and the *SCP*-α diagram is the loss of positional information of the spectra. In order to compensate for this weakness, we present the *SCP*-α diagram and the *SCP* map together. In this way, the position information of spectra can be restored. Some first results of this exercise will be shown in the next section.

3. Application to radio galaxies

In this section, we present *SCP*-α diagrams of three Giant Radio Galaxies (GRGs) and of a sample of Compact Steep Spectrum (CSS) sources. The integrated spectra have been analyzed by Mack et al. (1998) for GRGs and by Murgia et al. (1999) for CSS sources with synchrotron ageing models. Error bars in the diagrams are $\sigma_{\rm scp}$ and σ_α. These are estimated as shown below,

$$\sigma^2_{\rm scp} = \frac{4\left(\alpha^2_{\rm high}+\alpha^2_{\rm low}\right)}{\left(\alpha_{\rm high}+\alpha_{\rm low}\right)^4}\left(\alpha^2_{\rm high}\sigma^2_{\alpha_{\rm high}}+\alpha^2_{\rm low}\sigma^2_{\alpha_{\rm low}}\right)$$

$$\sigma_\alpha = 1/\log(\lambda_2/\lambda_1)\sqrt{\left(\sigma^2_{\rm I,1}/I^2_1\right)+\left(\sigma^2_{\rm I,2}/I^2_2\right)}.$$

$\alpha_{\rm low}$ and $\alpha_{\rm high}$ are the spectral indices ($I_\nu \propto \nu^{-\alpha}$), obtained at low (e.g. <1 GHz) and at high (e.g. >1 GHz) frequencies, respectively. Since two independent spectral indices are needed for the *SCP*, observations over at least three different frequencies are necessary.

3.1. Giant radio galaxies

These objects are classified by their projected linear sizes. The measurements used here have been performed by Mack et al. (1997) at frequencies between 326 MHz and 10.6 GHz. We use four frequencies in our analysis, viz. 326 MHz, 610 MHz, 4.8 GHz and 10.6 GHz. We compute $\alpha^{610\ \rm MHz}_{326\ \rm MHz}$ as $\alpha_{\rm low}$, and $\alpha^{10.6\ \rm GHz}_{4.8\ \rm GHz}$ as $\alpha_{\rm high}$. All maps were convolved to a common resolution of $150'' \times 150''$, *SCP*-α diagrams were produced for brightness levels above $\sim 3\sigma$. In general, the low–frequency spectral indices in the lobes of all three sources remain relatively constant, $\alpha_{\rm low} \sim \alpha_{\rm inj}$. This means that neither ageing processes nor synchrotron self–absorption play an important rôle at low frequencies in the regions of interest. In what follows, we shall discuss the results for the three GRGs investigated here in detail. For the best performance, if needed, the cubic convolution interpolation method with a value of -0.5 is used when regridding (Park & Schowengerdt 1983). The linear convolution interpolation shows marginal difference.

3.1.1. DA 240

The radio morphology of DA 240 is symmetric at low frequencies, but becomes increasingly asymmetric towards higher frequencies (Mack et al. 1997). At 326 MHz, DA 240 is seen as a "Fat Double". The SW fat lobe has disappeared at 10.6 GHz, forming an elongated edge-darkened FR-I-type lobe. On the contrary, the NE lobe maintains its "fat round" shape up to 10.6 GHz.

A fit to the *SCP*-α diagram yields steep injection spectra, $\alpha_{\rm inj} \sim 0.82$ (NE lobe) and ~ 0.94 (SW lobe). These unusually steep and asymmetric injection spectra have already been reported by Mack et al. (1998), viz. 0.76 and 0.97 for the NE and SW lobe respectively. Those authors used the synchrotron ageing technique. The difference of the injection spectral indices is relatively large in the NE lobe, since the region with *SCP* < 0 of the NE lobe (Fig. 4) is included in the integrated synchrotron ageing calculation. Including this flatter-spectrum region, $\alpha_{\rm high} = 0.5 \ldots 0.85$ makes the synchrotron ageing estimate uncertain. On the whole, our intuitive rapid estimation shows good agreement with their result.

Besides this asymmetry of the injection spectral indices, the two lobes reveal quite different trends in the diagram. The synchrotron ageing theory, the CI model and the KP/JP model, well describes the trend in the SW lobe (Fig. 5). The CI bifurcation is detected. On the other hand, the majority of the *SCP* values in the NE lobe are well below zero. This is a clear case of spectral flattening. The remaining points with *SCP* > 0 are best fitted by the CI model. In the NE lobe $\alpha_{\rm high}$ commences with 0.5, then increases to 0.8 below *SCP* < 0. This is indicative of a non-relativistic strong shock as discussed in the last section. Since there is no clue of KP bifurcation (see Fig. 1) or outreach of JP spectra on the *SCP*-α diagram, due to the sensitivity limit of the observation, we can not definitely prefer any model to the others, except for region CI mentioned in Fig. 5. Comparing Fig. 4 and Fig. 5, it is found that the projected position of the CI bifurcation is the channel of the brightness peak of the SW lobe to the SW extremity. This possibly indicates that the physical condition of CI model, namely continuous injected electrons with no significant escape, is yet valid in this region.

3.1.2. NGC 315

Spectral flattening is present over the whole source. The value $\alpha_{\rm inj} \sim 0.58$ in the NW lobe is consistent with the estimate of Mack et al. (1998), who obtained $0.54 \ldots 0.59$. On the other hand, we cannot properly estimate the injection spectral index of the SE lobe, due to the small number of points with *SCP* > 0 and the large uncertainties. The general trend in the SE lobe implies a steep injection spectrum, $\alpha_{\rm inj} \sim 1.0$. The trends in the two lobes are neither symmetric nor asymmetric, but rather symmetric w.r.t the minor-axis (Fig. 7). At the southern ends of the two lobes, the spectral-upturning is striking. After that, towards the north, a gradual steepening follows.

The tracks of the NW and the SE lobe are well separated, which implies different injection indices, although the error is quite large. The reason for the extremely flat and even upturning curvature in the NW is unclear. Unresolved background sources or relativistic shocks could be the explanation. Enßlin et al. (2001) suggest that the relic NW tail of NGC 315 is re-accelerated by a cosmological shock wave. Our analysis demonstrates that the particles in both lobes have been re-accelerated. If the re-acceleration scenario is true, the spectral flattening implies that the energy threshold of this acceleration and/or $B_{\rm sync}$ of this region are higher than those of the injection spectrum. Spectral flattening plus an upturn are independent from possible missing short-spacing problems

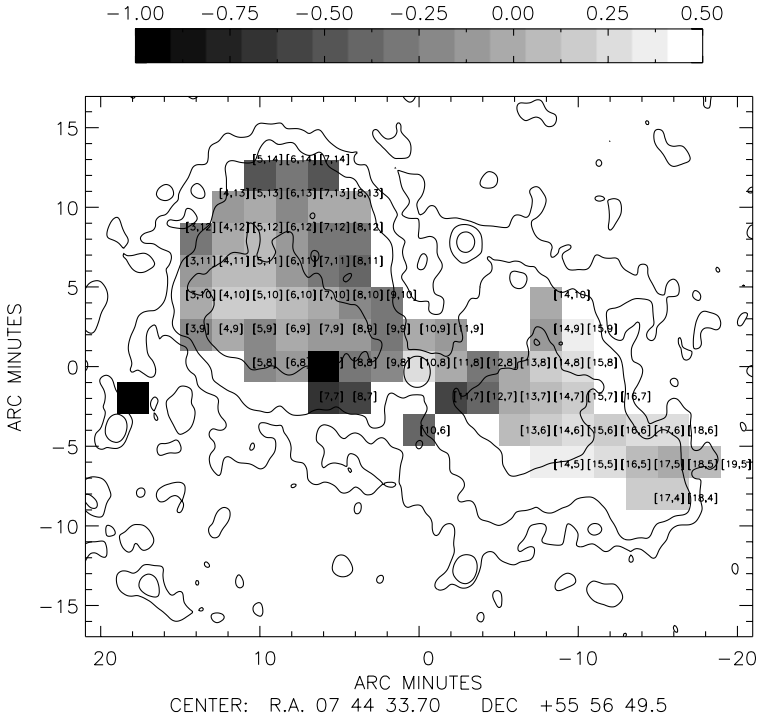

Fig. 4. *SCP* map of DA 240. The contours show the total intensities at 326 MHz (Mack et al. 1997). Contour levels are $3\sigma_I$, $10\sigma_I$ and $50\sigma_I$. The *SCP* map shows asymmetry. The spectral curvature of the NE lobe is nearly a power-law in the vicinity of its bright centre [5, 10]. The envelope of the NE lobe shows spectral flattening. This implies an effective in situ acceleration, possibly through the interaction with a surrounding thermal magneto-ionic medium whose existence is detected via its rotation measure (Sohn 2003). The *SCP* values of the SW lobe are in a range which is expected by the particle ageing theory. The SW lobe has no well-defined envelope at high frequencies. Its SW extremity shows spectral flattening with respect to its bright centre. The fact that all of DA240's extremities have a *SCP* flatter than their brightness centres implies that the interaction (i.e. re-acceleration) with its environment is an essential mechanism for the growth of this GRG.

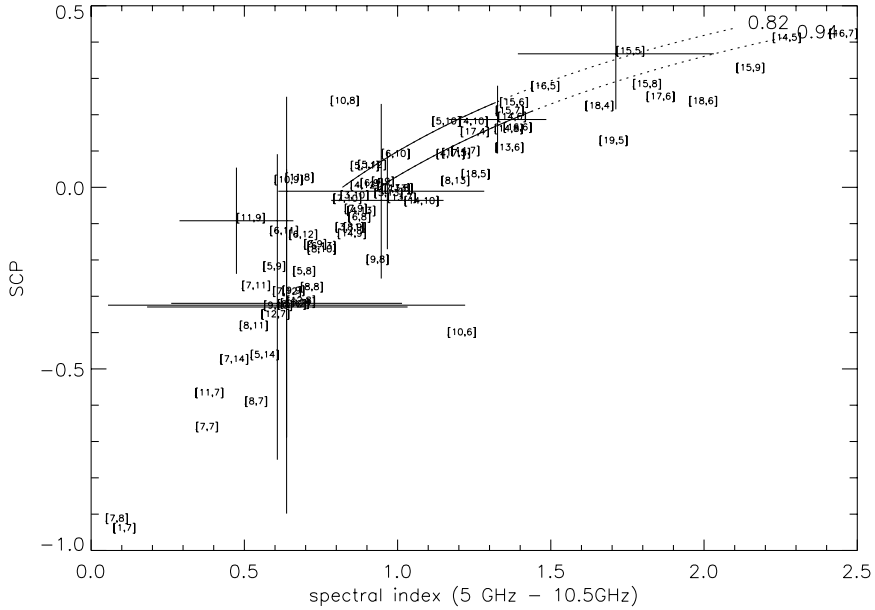

Fig. 5. *SCP*-α diagram of DA 240. The error estimation is described in the text. Two lines represent the best fit to the SW lobe and the NE lobe respectively. For the fitting procedure, only points with $SCP > 0$ of the each lobes were used. In the SW lobe, two interesting trends are visible. If we confirm the linear drop at the end of the CI track, with $\alpha_{\rm inj} \sim 0.82$, inspite of the large error of *SCP* and $\alpha_{\rm high}$, this can be interpreted as the CI bifurcation in Fig. 2. If this linear bifurcation is real, it implies that $B_{\rm sync}$ in the CI region is much stronger than $B_{\rm CMB}$. Otherwise the CI bifurcation is not seen clearly. The second points is the spread of data in the KP/JP range. Again inspite of the error bar, the trend visible here resembles the evolution of KP spectrum (see Fig. 18), and $B_{\rm sync}$ may be several times stronger than $B_{\rm CMB}$.

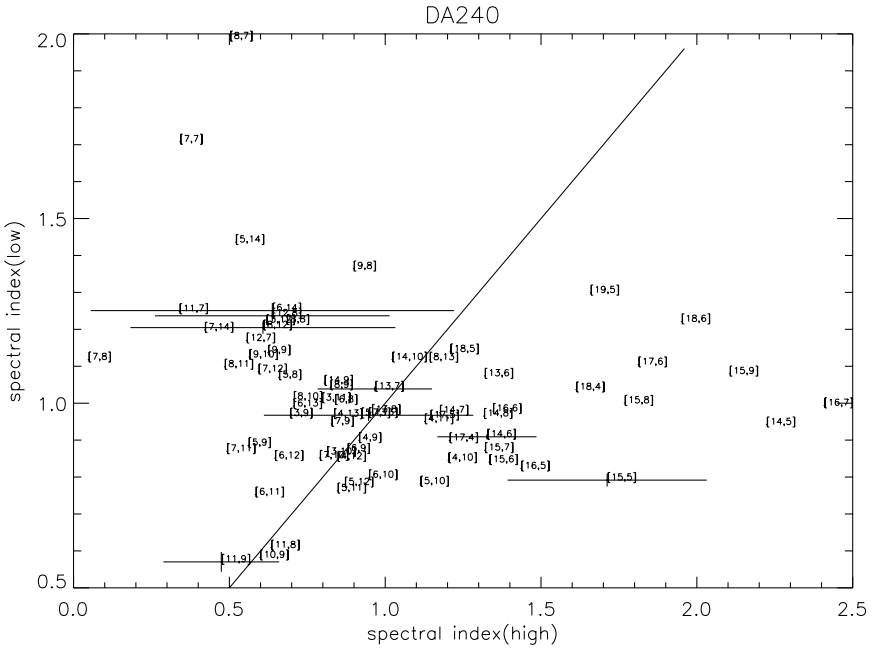

Fig. 6. C–C diagram of DA 240. The straight line corresponds to a pure power-law. The area to its left is populated by points of spectral flattening, the area to its right contains points which show spectral steepening.

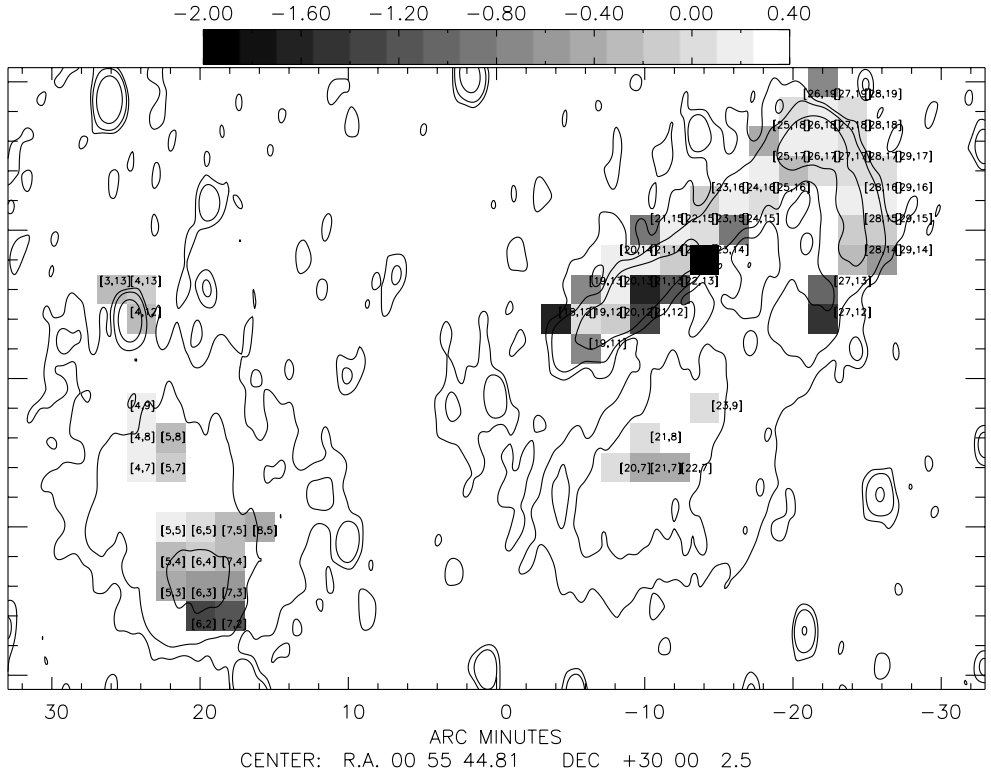

Fig. 7. *SCP* map NGC 315. Contours show the total intensities at 326 MHz Mack et al. (1997). Contour levels are $3\sigma_{\rm I}$, $10\sigma_{\rm I}$ and $50\sigma_{\rm I}$. Although its morphology is highly asymmetric, there is no significant spectral asymmetry along the major jet axis. Along the minor axis, in the SW to NE direction, the spectral curvature exhibits gradual steepening. This is clear in the whole SEern lobe and in the bow structure of NWern lobe. The relic tail of this structure also has flat spectral curvature.

inherent to the 610 MHz WSRT data, since it would be detectable via the Effelsberg single dish multi-frequency observations at 2.6, 4.8 and 10.6 GHz (Mack et al. 1998) alone. However the prominence of the points with $SCP < 0$ could be correlated with the angular size of the 610 MHz data. It can be speculated that this is a viable explanation for the prominence of $SCP < 0$ in NGC 315, which is by far the largest source in terms of angular size, $\Phi \sim 1$ deg. On the other hand, a value α

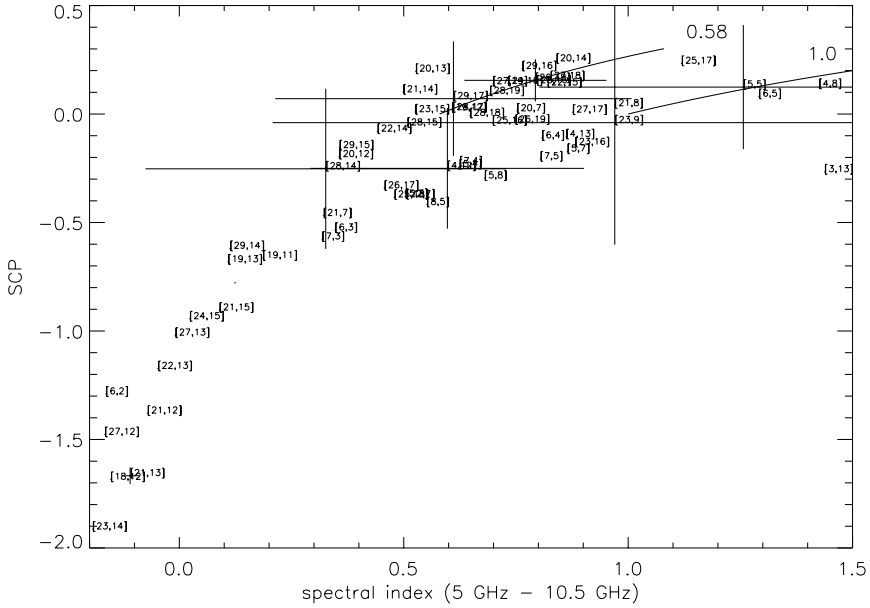

Fig. 8. *SCP-α* diagram of NGC 315. The *SCP* values are curiously flat in the source. The main jet to the NW end has a low injection index, $\alpha_{\rm inj} \sim 0.58$. $\alpha_{\rm inj}$ of the NWern relic tail and the SEern lobe is rather high, ∼1. The NWern relic and the SEern lobe possibly have the same particle re-acceleration history.

of our *SCP–α* diagram is also obtained from single-dish 4.8 and 10.6 GHz data and shows $\alpha < \alpha_{\rm inj}$. The spectral flattening in NGC 315 is mainly because of a low $\alpha_{\rm high}$.

3.1.3. 3C 236

This source is the largest known GRG, with $d \sim 4.5$ Mpc. It has a typical FR II morphology. Our value of $\alpha_{\rm inj}$ of 0.7 in the SE lobe (Fig. 11) is in the range of the integrated synchrotron ageing estimate of 0.5 to 0.7 by Mack et al. (1998). In the NW lobe, we obtain a steep $\alpha_{\rm inj}$ of 1.10. The integrated spectral index from synchrotron ageing theory for this lobe is 0.7.

The spectral flattening shown at the extremity of the SE lobe is due to a known background source (Mack et al. 1997). In the NW lobe, we find two different values of $\alpha_{\rm inj}$, without any significant flattening. One of them is well fitted by a steep spectrum, $\alpha_{\rm inj} \sim 1.10$. The trend of these data clearly shows the synchrotron ageing in the lobe. In the backflow or so-called bridge region, $\alpha_{\rm inj} \sim 0.7$ yields the best fit. Such an injection discrepancy between hot-spots and lobes has been reported for Cygnus A (Carilli et al. 1991). The injection spectral indices of the hot spots and lobes of Cygnus A are 0.5 and 0.75, respectively. The difference $\Delta\alpha_{\rm inj} \sim 0.4$ here is larger than in Cygnus A. In Cygnus A, the hot-spots have $\Delta\alpha_{\rm inj} \sim 0.25$ flatter than their lobes, i.e. their backflows. 3C 236 has a steeper spectrum ($\alpha_{\rm inj}$) in the advancing region. An explanation for this $\alpha_{\rm inj}$ discrepancy (Carilli & Barthel 1996) has not been found so far.

3.2. CSS sources

SCP-α diagrams can also be used for the analysis of samples of sources for which only integrated flux densities are given. As an example we present the application of our method to a sample of 47 Compact Steep Spectrum (CSS) sources. Murgia et al. (1999) who have analyzed the flux densities of a sample of CSS sources in a profound synchrotron ageing study show that these sources have moderate spectral steepening, i.e. a difference of $\Delta\alpha \sim 0.5$ between low- and high-frequency spectral indices, which is predicted by the continuous injection model (CI). We have used this sample to test the *SCP* performance, which provides an alternative method for a quick analysis of synchrotron spectra. In essence, four frequencies 408(327) MHz, 1.4 GHz, 4.9(5.0) GHz and 10.7(10.6, 8.1) GHz, were used. When no data were available at these frequencies, the total intensity at the frequencies given above in the brackets were taken.

The points are found in the region where $\alpha_{\rm high}$ does not exceed $\alpha_{\rm inj} + 0.5$. The obtained range of $\alpha_{\rm inj}$ values is rather wide. This confirms the results of Murgia et al. (1999). The fact that $\alpha_{\rm inj}$s shows more scatter in the *SCP-α* analysis than in the synchrotron model estimation is due the effect synchrotron self-absorption. There is a clear trend that the sources with stronger $B_{\rm eq}$ and with smaller projected sizes have flatter $\alpha_{\rm inj}$. These are the compact GHz-Peaked Spectrum (GPS) source candidates, since due to their extreme compactness $d \leq 1$ kpc, synchrotron self-absorption is liekly to be effective. The sample does not shows any correlation with redshift. This implies that the intrinsic magnetic fields proponder by far over the magnetic field equivalent to the cosmic microwave background.

4. Discussion

The above analysis implies that all studied sources have a complex history. Now we discuss some possibilities. Before attempting any physical interpretation, we check again whether *SCP* ~ -1 could be generated by the possible missing short-spacing at 610 MHz. If anything, the possible missing

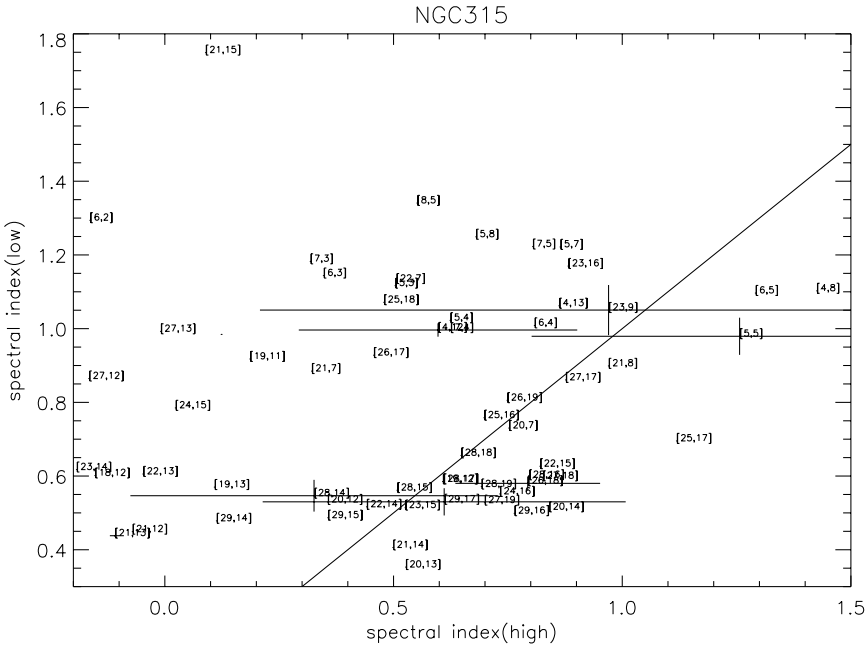

Fig. 9. C–C diagram of NGC 315 (see Fig. 6).

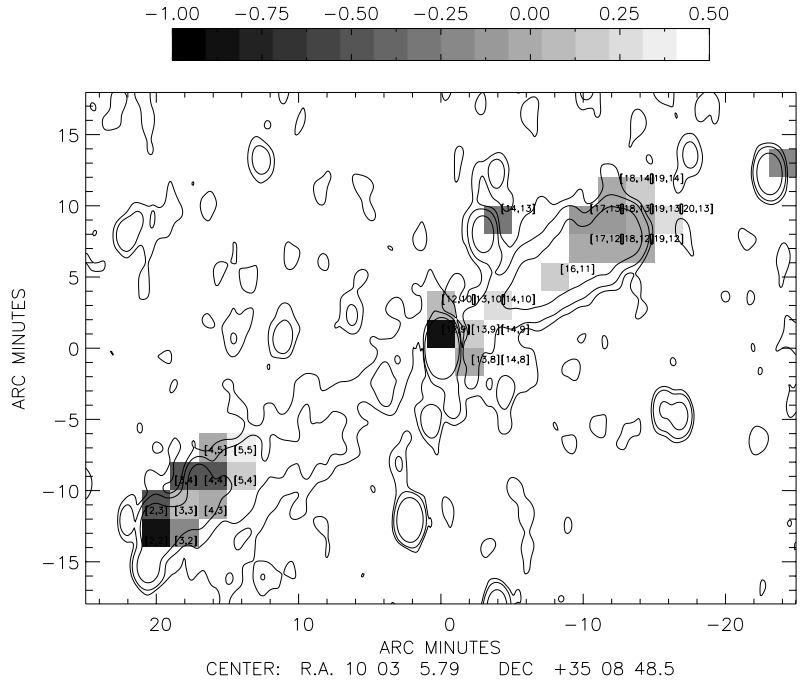

Fig. 10. *SCP* map of 3C 236. The contours show the total intensities at 326 MHz Mack et al. (1997). Contour levels are $3\sigma_{\rm I}$, $10\sigma_{\rm I}$ and $50\sigma_{\rm I}$. Two lines are the best fit results for the NW lobe and the SE lobe, respectively. The very flat SE extremity of *SCP* is due to a background source (Mack et al. 1998). The central core undergoes strong self-absorption, *SCP* < 0. In general, *SCP* is symmetric in 3C 236.

short spacing at 610 MHz will steepen our $\alpha_{\rm low}$, which is already >0. Then,

$$SCP = \frac{\alpha_{\rm high} - \alpha_{\rm low}}{\alpha_{\rm high} + \alpha_{\rm low}} \sim -1, \alpha_{\rm low} > 0.$$

This is possible, if $\alpha_{\rm low} \gg \alpha_{\rm high}$ or $\alpha_{\rm high} \sim 0$. $\alpha_{\rm low} \gg \alpha_{\rm high}$ is not known. The $SCP < 0$ trend can be emphasized, when $\alpha_{\rm low} > \alpha_{\rm high}$ and $\alpha_{\rm high} < 1$ are working together. But again the measured $\alpha_{\rm low}$ alone cannot explain the flattening up to $SCP \sim -1$. The trends in the sources are mainly due to the high-frequency curvature, $\alpha_{\rm high}$.

4.1. Expansion loss, energy cut–off and synchrotron self–absorption

Adiabatic expansion losses may play an important role as an energy loss process of synchrotron sources. However,

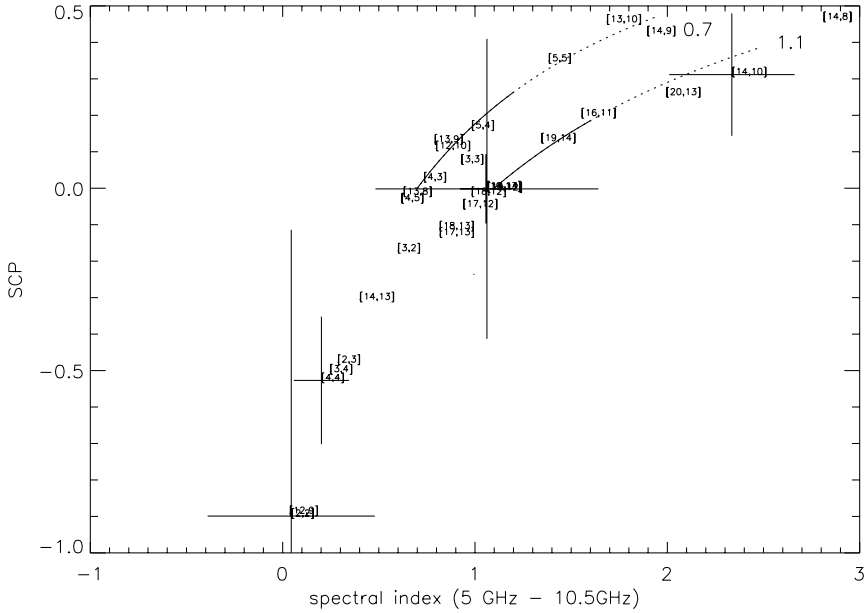

Fig. 11. *SCP-α* diagram of 3C 236. Except for the central core and the background source, the points are well fit by two values of $\alpha_{\rm inj}$. The SE lobe has $\alpha_{\rm inj} \sim 0.7$. In the NW lobe, two values of $\alpha_{\rm inj}$s are seen. The near-to-core bridge has $\alpha_{\rm inj} \sim 0.7$, just like the SE lobe. The NW outer lobe has a much steeper $\alpha_{\rm inj} \sim 1.1$.

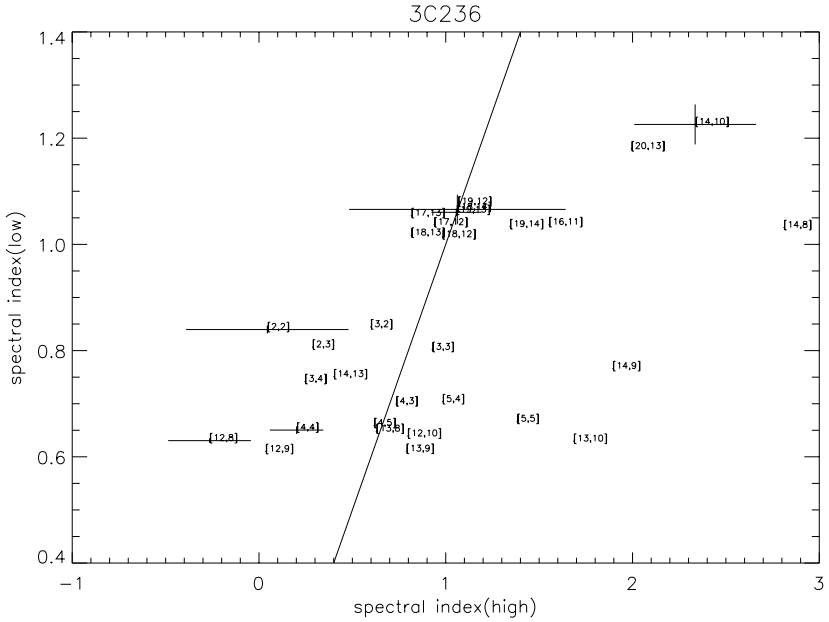

Fig. 12. C–C diagram of 3C 236 (see Fig. 6).

as Carilli et al. (1991) already pointed out, although adiabatic expansion will shift the spectral break to lower frequencies, the expansion does not change the spectral curvature. Therefore, expansion losses will not affect the tracks of *SCP–α*.

At low frequencies, there are also other physical processes that give rise to spectral curvature, such as spectral turn-overs by synchrotron self-absorption in regions of high particle densities, or by a low-energy cut-off in the particle distribution. In the *SCP–*$\alpha_{\rm high}$ plane (Fig. 2), the low-frequency turn-over produces $SCP > 1$, which cannot be produced by any ageing processes. Strong self–absorption can even produce $SCP < 0$ and will be important in the central core regions, if $|\alpha_{\rm low}| > |\alpha_{\rm high}|$. Since $\alpha_{\rm low}$ will eventually approach $-5/2$ in the Rayleigh–Jeans limit, this will be possible.

4.2. Re-acceleration

All three GRGs exhibit spectral flattening in some parts. In particular, NGC 315 even shows signs of a spectral up–turn at high frequencies, and the majority of *SCP* points is under 0. Let us

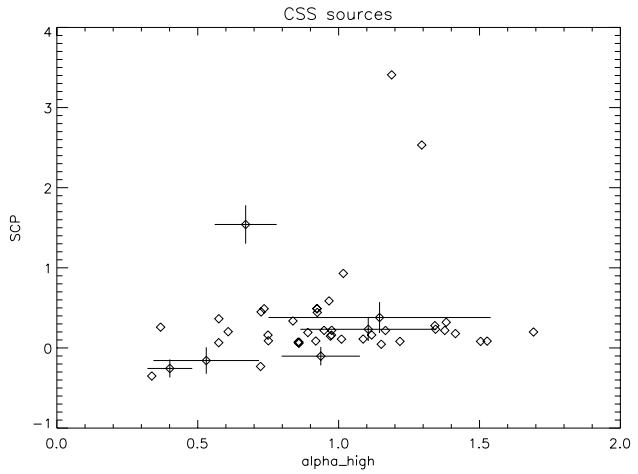

Fig. 13. *SCP*-α diagram for 47 CSS sources. 40 sources have *SCP* values between 0 and 1. $SCP > 1$ clearly implies synchrotron self-absorption (see Fig. 2) at low frequencies. 3 out of 47 sources have $SCP > 1$. Due to the apparent synchrotron self-absorption at low frequencies, these sources were excluded from the further analysis in this work.

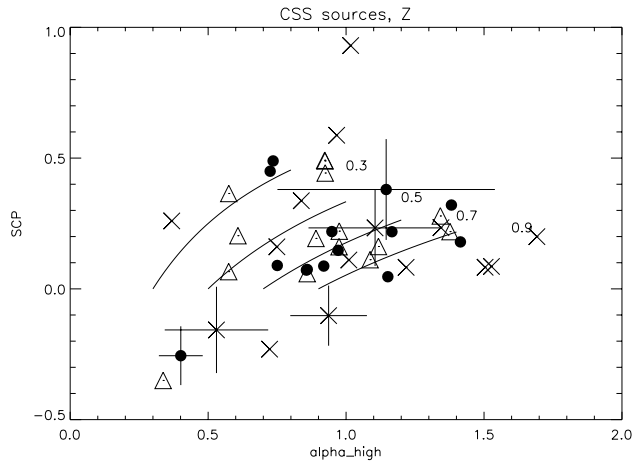

Fig. 14. Filled circles are CSS sources with $z < 0.5$. Open triangles are CSS sources with $0.5 \leq z < 1.0$. Crosses are CSS sources with $z \geq 1.0$. The sample does not show any *z*-related trend in the *SCP*-α diagram.

consider the case where the power-law injection spectrum is already established,

$$N(E) \propto E^{-p}, \alpha_{\rm inj} = (p-1)/2$$

and where Fermi acceleration is working. By the Fermi process, the particles in each energy bin will be re-accelerated such as to yield a power-law of the form $N(E) \propto E^{-q}$. For the non-relativistic strong shock, $q = 2$. The final shape of these two power laws is described by the following integration:

$$N(E) \propto E^{-q} \int_{E_0}^{E} E'^{-p} E'^{q-1} {\rm d}E',\ q > 1,\ p > 1$$

where E_0 is low energy cut off. This can be approximated (Blandford & Eichler 1987; Eilek & Hughes 1991; Sohn 2003).

(i) for $q < p$, $N(E) \propto E^{-q}$, $\alpha = (q-1)/2$
(ii) for $p < q$, $N(E) \propto E^{-p}$, $\alpha = (p-1)/2$.

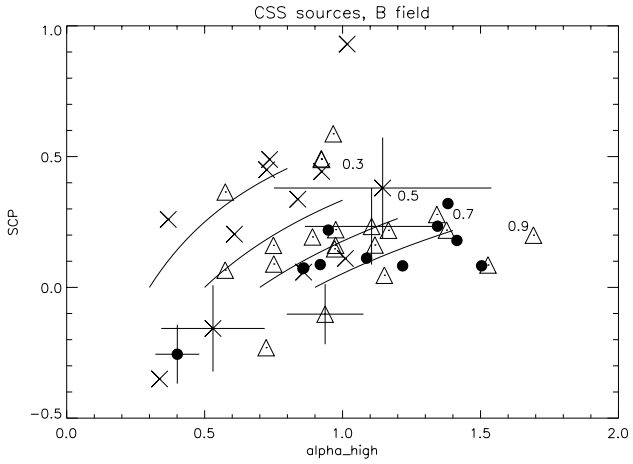

Fig. 15. Filled circles are CSS sources with $B_{\rm eq} < 5 \times 10^2$ μG. Open triangles are CSS sources with 5×10^2 $\mu{\rm G} \leq B_{\rm eq} < 10^3$ μG. Crosses are CSS sources with $B_{\rm eq} \geq 10^3$ μG. $B_{\rm eq} \geq 10^3$ μG sources have flatter spectral curvature than the weaker $B_{\rm eq}$ CSS sources. $B_{\rm eq} \sim 10^3$ μG is typical value for GPS sources. GPS sources have their turn-over (due to synchrotron self-absorption) at GHz frequencies. Their $\alpha_{\rm low}$s are flat, $\alpha_{\rm low} < \alpha_{\rm inj}$, since they are estimated at <1 GHz. The lines in the diagram were drawn assuming $\alpha_{\rm low} \geq \alpha_{\rm inj}$. As the result GPS sources tend to have flat $\alpha_{\rm inj}$, <0.5. Some CSS sources have flat $\alpha_{\rm inj}$ (Murgia et al. 1999) indeed, but these are not directly related to GPS sources, and none of them has extremely flat $\alpha_{\rm inj} < 0.3$.

In case (i), spectral flattening and $SCP < 0$ is expected (Fig. 2). An interesting result is that not every effective Fermi process results in a spectral flattening. In case (ii), the source will just look younger than indicated by its kinematic age, inferred from the shift of the break frequency towards higher frequencies (Parma et al. 1999). There is no flattening, since the energy distribution of the re-accelerated particles follow $N(E) \propto E^{-p}$, not E^{-q}.

Since GRGs are extraordinary extended, they should have a weak magnetic field $\leq B_{\rm CMB}$ (Mack et al. 1998) and/or undergo re–acceleration processes during in their lifetime.

Considering the confusion of spectra of different components with different spectral indices the observed high frequency spectral flattening indicates that the flatter spectrum component is younger and secondary, i.e. re–accelerated. Otherwise we would not see the high frequency flattening, if the flatter spectrum component is as old as the steeper spectrum component. Or if the flatter spectrum component is dominant, then we would see only the flatter spectrum component in the radio frequency range and then there would be no spectral flattening.

4.3. (Equivalent) Magnetic fields

The magnetic field $B_{\rm sync}$ and the equivalent field of the cosmic microwave background, $B_{\rm CMB}$ determine the curvature beyond $\nu_{\rm br}$. In some models (e.g. Eilek & Arendt 1996) magnetic fields produce a power-law spectrum when they are ordered in a power-law form. However, we restrict our discussion to the curvature beyond $\nu_{\rm br}$, and to a simple homogeneous magnetic field $B_{\rm sync}$ plus $B_{\rm CMB}$. Many radio galaxies as well as

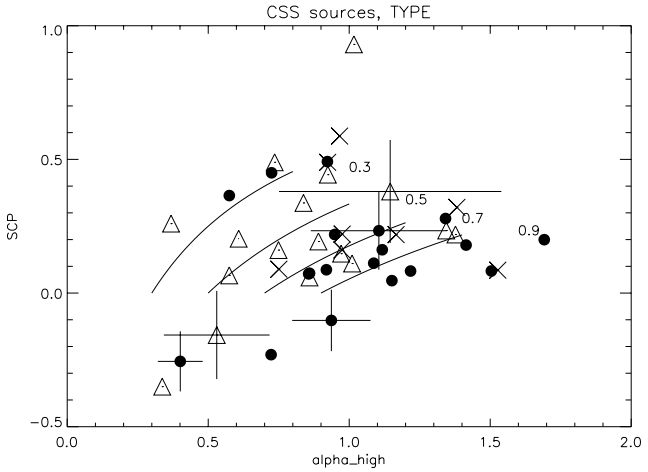

Fig. 16. Filled circles are *lobe dominated* CSS sources. Open triangles are *core dominated* CSS sources. Crosses are uncertain types of CSS sources. There is no clear trend to distinguish the three classes in the diagram. It can be partly due to the fact that CSS sources and GPS sources are not a proper definition of source morphology, but of rather represent an evolutonary stage (visible in their spectrum). Relatively nearby GPS sources can be resolved and defined as *lobe dominated*, while distant CSS sources can be unresolved and defined as *core dominated*. Alternatively, some "frustration scenario" could be working. A definite answer would be only possible with the improvement of VLBI imaging.

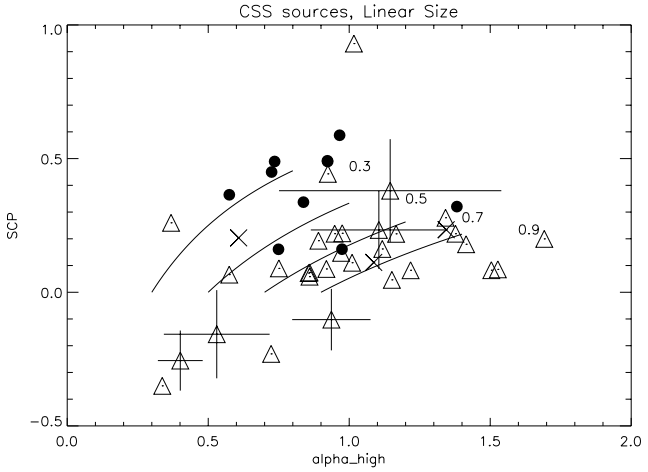

Fig. 17. Filled circles are $d < 1$ kpc sources. Open triangles are $1 \leq d < 10$ kpc sources. Crosses are $d \geq 10$ kpc sources. Projected linear size, d, classes exhibit clear grouping of CSS sources as in $B_{\rm eq}$ class. GPS sources are typically smaller than 1 kpc.

GRGs have weak magnetic fields (Feretti et al. 1998; Mack et al. 1998; Parma et al. 1999), assuming that the equipartition estimation yields the strength of the magnetic field of the radiation region, $B_{\rm eq} = B_{\rm sync}$. The JP model becomes more appealing since it allows for pitch angle isotropization on a much shorter time scale than the radiation lifetime, $\tau_{\rm iso} \ll \tau_{\rm sync}$. However, KP "like" spectra are observed (e.g. Carilli et al. 1991). In order to explain such KP spectra, variable $B_{\rm sync}$ fields were introduced (Tribble 1993; Eilek et al. 1997). In Tribble's model, the magnetic field has a Maxwellian distribution, while in Eilek's model, magnetic fields are filamented, therefore have

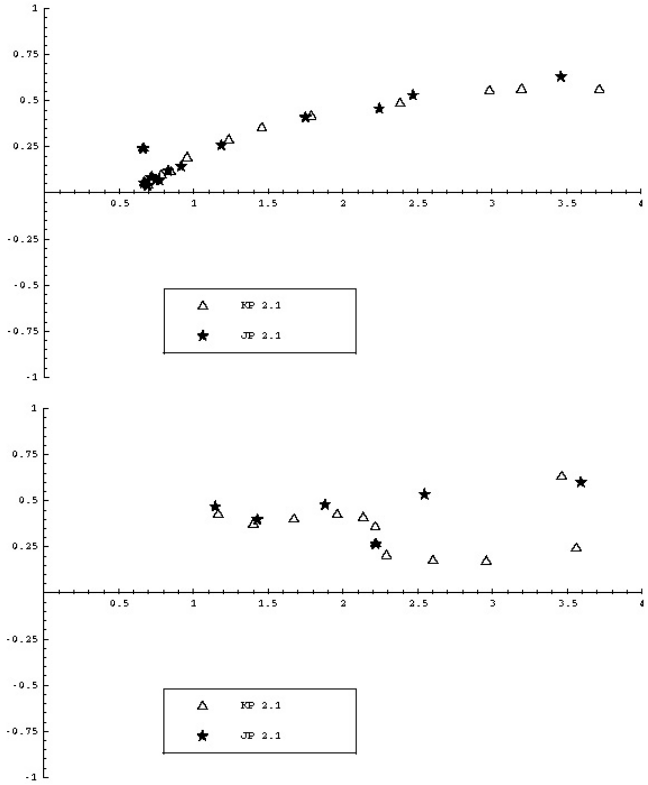

Fig. 18. Comparison of KP and JP spectra under $B_{\rm CMB} = 3$ μG.The abscissa is $\alpha_{\rm high}$ and the ordinate is *SCP*. The frequency intervals were selected to be similar to the observating frequencies of the GRGs. In the simulation synchrotron losses, $IC_{\rm CMB}$ losses and slight energy cut–off effects are considered. From top to bottom, the magnetic field $B_{\rm sync}$ is given as 6 μG and 15 μG. Age, power index, $p = 2.1(\alpha_{\rm inj} = 0.55)$, and $B_{\rm CMB} = 3.2$ μG are the same in all three diagrams. The pitch angle argument which makes the KP spectrum and the JP spectrum different is only valid when $B_{\rm sync}$ is distinctively stronger than $B_{\rm CMB}$. The bifurcation predicted in Fig. 1 is seen in the $B = 15$ μG diagram, while beyond that KP also has an asymptotic tail, since in the end the effect of $B_{\rm CMB}$ appears. This will happen at a very steep $\alpha_{\rm high} > 2.5$.

approximately two components, $B_{\rm strong}$ and $B_{\rm weak}$. But again, any of these models requires that some portion of their B fields is stronger than the equivalent $B_{\rm CMB}$ to such as to produce the KP-like spectrum.

In any case, KP–like spectra are only possible when there is a strong magnetic field, with respect to $B_{\rm CMB}$. Therefore, the existence of KP spectra indicates that synchrotron radiation is the most important energy loss process in the region considered here. Furthermore, the variation of $B_{\rm sync}$, if any, will cause a broadening of the spectral turn-over at low frequencies.

5. Summary and conclusions

We have investigated an alternative and very efficient method for the analysis of synchrotron spectra. We apply it both, to extended sources (like GRGs) and to the integrated flux densities of a sample of CSS sources. For all of them a thorough synchrotron ageing study has been performed which can be used for comparison. The information obtained from the spectral curvatures is manifold. The hot spots and jets possess pure

power-law spectra, with particle ageing as expected. The spectral curvatures of the lobes exhibit both, spectral steepening and flattening.

In DA 240, there are CI spectra at the SW extremity, while KP/JP spectra show up around the bright core of the SW lobe. We cannot find any bifurcation in the diagram, which serves as the definite distinction between the KP model and the JP model. More sensitive and/or higher-frequency observations are needed to reveal the bifurcation between the KP and JP models as shown between CI and KP/JP in DA 240. If a KP bifurcation is seen, it can be interpreted as an identification of the existence of a strong $B_{\rm sync}$, i.e. $B_{\rm sync} > B_{\rm CMB}$. As seen in Fig. 18, KP spectra can be identified. Otherwise, the spectra would look like JP spectra, due to the influence of the isotropic nature of $B_{\rm CMB}$.

The high-frequency spectral indices start at values of around 0.5, which is indicative of non-relativistic strong shock acceleration. A possible origin of the shock could be the interaction of radio galaxies with their surrounding IGM/ICM (e.g. Enßlin et al. 2001). Adiabatic expansion, the other significant energy loss process, does not affect the *SCP*-α diagram. The results demonstrate that the *SCP* provides crucial parameters for the continuum spectrum of synchrotron radiation, without the more complex modeling.

Three characteristics that we have found in GRGs are not yet explained. The first is the origin of the asymmetry of the injection spectra of the radio lobes. Second, the physical explanation of the systematic flattening of $\alpha_{\rm high}$ compared to $\alpha_{\rm inj}$ is unknown. Third, there is a critical change of the re-acceleration efficiency showing up in the low- and high-frequency regime. We will investigate the environments of GRGs to find the possible reason.

In conclusion, it can be stated that the *SCP*-α diagram proves to be an efficient method to derive important properties of synchrotron spectra which otherwise can be determined only with the much more complex synchrotron ageing analysis. The *SCP*-α diagram and *SCP* map are especially useful to analyze a large number of sources and a large number of spectral points in a source. In those cases, the complex spectral analysis will give better estimation. However, this alternative tool provides fast estimates without losing accuracy significantly and provides an overview which is important to understand synchrotron sources. Compared to the C–C diagram, the *SCP*-α diagram extracts injection spectral indices and possible synchrotron ageing models in a source more efficiently.

Acknowledgements. BWS is grateful to Heino Falke for discussions of the various shock acceleration conditions. KHM was supported by a Marie-Curie Fellowship. The authors are grateful to the anonymous referee for her/his fruitful comments.

References

Alexander, P. 1987, MNRAS, 225, 27
Alexander, P., & Leahy, J. 1987, MNRAS, 225, 1
Blandford, R., & Eichler, D. 1987, Phys. Rev., 154, 1
Carilli, C., & Barthel, P. 1996, A&A, 7, 1
Carilli, C., Perley, R., Dreher, J., et al. 1991, ApJ, 383, 554
Eilek, J. A., & Arendt, P. 1996, ApJ, 457, 150
Eilek, J. A., & Hughes, P. 1991, Beams and Jets in Astrophysics (Cambridge Univ. Press)
Eilek, J. A., Melrose, D., & Walker, M. 1997, ApJ, 483, 282
Enßlin, T., Simon, P., Biermann, P., et al. 2001, ApJ, 549, L39
Feretti, L., Giovannini, G., Klein, U., et al. 1998, A&A, 331
Jaffe, W., & Perola, G. 1973, A&A, 26, 423
Kardashev, N. 1962, Soviet Astron., 6, 317
Katz-Stone, D., & Rudnick, L. 1994, ApJ, 426, 116
Katz-Stone, D., & Rudnick, L. 1997, ApJ, 488, 146
Katz-Stone, D., Rudnick, L., & Anderson, M. 1993, ApJ, 407, 549
Klein, U., Mack, K.-H., Gregorini, L., et al. 1995, A&A, 303, 427
Mack, K.-H., Klein, U., O'Dea, C., et al. 1997, A&AS, 123, 423
Mack, K.-H., Klein, U., O'Dea, C., et al. 1998, A&A, 329, 431
Murgia, M., Fanti, C., Fanti, R., et al. 1999, A&A, 345, 769
Pacholczyk, A. 1970, Radio Astrophysics (San Francisco: Freeman)
Pacholzcyk, A. 1977, Radio Galaxies (Oxford: Pergamon press)
Park, S., & Schowengerdt, R. 1983, Graphics & Image Processing, 23, 256
Parma, P., Murgia, M., Morganti, R., et al. 1999, A&A, 344, 7
Sohn, B. 2003, Ph.D. Thesis, Univ. Bonn
Tribble, P. 1993, MNRAS, 261, 57